Available online at www.sciencedirect.com
SCIENCE DIRECT
Physics Letters A 356 (2006) 35–43
PHYSICS LETTERS A
www.elsevier.com/locate/pla

Chaos synchronization of two stochastically coupled random Boolean networks

Yao-Chen Hung [a,b,*], Ming-Chung Ho [b], Jiann-Shing Lih [c,b], I-Min Jiang [a,b]

[a] *Department of Physics, National Sun Yat-sen University, Kaohsiung, Taiwan*
[b] *Nonlinear Science Group, Department of Physics, National Kaohsiung Normal University, Kaohsiung, Taiwan*
[c] *Department of Physics & Geoscience, National Pingtung University of Education, Pingtung, Taiwan*

Received 5 November 2005; received in revised form 2 March 2006; accepted 9 March 2006

Available online 22 March 2006

Communicated by C.R. Doering

Abstract

In this Letter, we study the chaos synchronization of two stochastically coupled random Boolean networks (RBNs). Instead of using the "site-by-site and all-to-all" coupling, the coupling mechanism we consider here is that: the nth cell in a network is linked by an arbitrarily chosen cell in the other network with probability ρ, and it possesses no links with probability $1-\rho$. The mechanism is useful to investigate the coevolution of biological species via horizontal genetic exchange. We show that the density evolution of networks can be described by two deterministic coupled polynomial maps. The complete synchronization occurs when the coupling parameter exceeds a critical value. Moreover, the reverse bifurcations in inhomogeneous condition are observed and under our discussion.

PACS: 02.50.-r; 05.45.Xt; 05.65.+b

Keywords: Boolean networks; Stochastic coupling; Synchronization

1. Introduction

Cellular automata are discrete dynamical systems which can exhibit complex special-temporal behaviors [1–3]. Besides the convenient and easy calculating procedure, the models give us good explanations of the microscopic mechanisms that lead to the macroscopic behavior of the systems. They provide simplified models for a wide variety of physical systems [4,5], such as magnetization in solids [6], reaction–diffusion processes [7], fluid dynamics for complex situations [8], growth phenomena [9], traffic flow models [10,11], and so on. Though a cellular automaton illustrates a relatively simple sketch of a real system, it still can grasp the typical and significant characteristics of the system it models. Therefore, it is important to investigate the dynamics of CA for realization and prediction in real systems.

Based upon the different evolution patterns, Wolfram separated all the rules of elementary cellular automata (ECA) into four classes: homogeneous state (class I), separated simple stable or periodic structures (class II), chaotic pattern (class III) and complex localized structures (class IV) [1–3]. The state of a cell is determined by the cell itself and its nearest two cells. The evolution rule of ECA can be described by the Boolean function: $c_n(t+1) = f_n[c_{n-1}(t), c_n(t), c_{n+1}(t)]$, where n is the site index and the up-date rule f is identical for each cell. Because ECA have a spatial structure, they can be applied to investigate one-dimensional crystal growth and fluid flow. However, when spatial locations are less meaningful, such as spin models with disordered long-range interaction, the problem of cell differentiation, and biological evolution, the Kauffman networks (KNs) are more suitable to model the systems than ECA [12,13]. This is because KNs are not arranged in any spatial structure and the up-date rule can vary from one cell to another. Actually,

* Corresponding author.
E-mail addresses: d9123801@student.nsysu.edu.tw (Y.-C. Hung), t1603@nknucc.nknu.edu.tw (M.-C. Ho).

0375-9601/$ – see front matter
doi:10.1016/j.physleta.2006.03.025

ECA can be regarded as a special case of KNs with connections $k = 3$, but the choice of an evolution rule and connections is deterministic. The dynamics of KN have been widely studied, and the details can be reviewed in Refs. [14–16].

There is an intermediate automaton between ECA and KN, which is called random Boolean network (RBN) or disordered cellular automaton (DCA). The connections of the RBNs are still randomly chosen but the evolution rules are identical for all cells (nodes) [17]. Unlike ECA and KNs, the dynamics of RBNs are still far less understood. Recently, Andrecut and Ali show that the RBNs obeying the generalized rule 126 for ECA can be exactly described by a density map [18]. The authors consider a simple Boolean network with N cells in which each cell is connected to k random chosen cells and the parameter k is known as the connectivity of the network. The value of k is fixed, and the state of each cell is influenced only by the cell itself and the k connections. The density map, which represents the probability of finding a cell in state 1 at time t, exhibits extremely abundant chaotic dynamics. Matache and Heidel extended the ideas to a more general condition: the connections k of one cell are different from another in the identical network [19]. Moreover, the authors consider that the model allows an asynchronous update rule for the N cells (ARBNs and GARBNs) [20]. These works are important in modeling real systems composed of multiple interacting components; notwithstanding the inherent interests in the problems themselves.

In this Letter, we study the coevolution dynamics, especially the chaos synchronization, in two coupled RBNs. Since the study from Pecora and Carroll [21], the investigation of synchronization has attracted a lot of attentions [22–25]. Although globally coupled chaotic oscillators with lower dimensions have been extensively studied, synchronization of spatially extended systems is still unexplored, particularly KNs and RBNs. One of the principal causes is their discrete characteristic of states which results in the uselessness of deterministic coupling. To solve the problem, Morelli and Zanette introduced a significant coupling method [26,27]. Because the coupling method is characterized by a probability g, it is called stochastic coupling mechanism. The mechanism has been applied to couple ECA, KNs, and RBNs successfully [26–28]. However, in addition to several special cases [29], the "site-by-site and all-to-all" coupling (that is, the nth cell in a network is connected restrictively to the nth one in the other network) is rarely seen in real systems. Here, we modify the coupling method to couple two RBNs: the nth cell in a network is linked by an arbitrarily chosen one in the other network with probability ρ, and it possesses no links from other cells with probability $1-\rho$. The mechanism is useful to investigate the panmictic population structures which results from "horizontal" exchange of genetic material between biological species [30]. It would also be helpful to investigate the dynamics of coupled gene networks [31]. Though the networks are stochastically coupled, our results show that two deterministic coupled polynomial maps can accurately describe their density evolution after statistic calculations. This outcome is important because the model provides good predictions of original networks and allows analytical calculations. Based upon the numerical simulations, we will represent the excellent match between the model and the original networks.

The inhomogeneous condition is also under our discussion. The inhomogeneity appears here in the form of different values of connectivity in different networks. Such inhomogeneous concept has been extended to study spinning control of spatiotemporal chaos [32], spatiotemporal intermittency dynamics [33], and phase synchronization (PS) phenomena [34] in coupled maps lattice. In this Letter, we observe the interesting reverse bifurcations via period-halving in inhomogeneous condition [19]. The mechanism is analyzed further in the text.

This Letter is organized as follows. In Section 2, we introduce a model of two coupled random Boolean networks and provide the deterministic coupled maps to model them. Numerical results show the excellent agreement between the original system and the model. In Section 3, we investigate the synchronization phenomena of coupled networks and analyze it by using mean-square error (MSE) and Lyapunov exponents. In Section 4, the reverse bifurcations in inhomogeneous condition are under our analysis. Finally, a brief conclusion and further works are given.

2. The deterministic coupled model

Let us consider two discrete networks with N cells individually. Each cell c_n^i, where $i = 1, 2$ indicates network 1 or network 2 and $n = 1, 2, \ldots, N$, is described by a Boolean variable 1 or 0. Suppose that two operators $\hat{\mathbf{R}}$ and $\hat{\mathbf{S}}$ govern the dynamics of coupled networks:

$$\mathbf{c}^{1,2}(t+1) = \hat{\mathbf{S}} \circ \hat{\mathbf{R}}\big(\mathbf{c}^{1,2}(t)\big), \tag{1}$$

where all cells update their states synchronously. The operator $\hat{\mathbf{R}}$ is the evolution rule of individual network. It is applied to both networks as they are not coupled. The coupling scheme we consider here is that: the cell c_n^1 (c_n^2) is linked by an arbitrarily chosen one c_m^2 (c_m^1) with probability ρ ($0 \leqslant \rho \leqslant 1$), and it possesses no links form other cells with probability $1-\rho$. The linkages are redetermined at each time step. Operator $\hat{\mathbf{S}}$ is the process of information exchange between networks, which compare and alter the states of linked cells in each network. Taking the network 1 into consideration, if c_n^1 possesses no links form other cells, c_n^1 will stay invariant after being operated by $\hat{\mathbf{S}}$. If cell c_n^1 is linked from c_m^2 and $c_n^1(t) = c_m^2(t)$, c_n^1 will not change. If cell c_n^1 is linked from c_m^2 and $c_n^1(t) \neq c_m^2(t)$, the coupling will not act and c_n^1 will not change with the probability $1-g$ ($0 \leqslant g \leqslant 1$) or the state c_n^1 will be c_m^2 with the probability g. Thus, the stochastic coupling scheme can be expressed as

$$\hat{S}_n\big(\mathbf{c}^1\big) = \begin{cases} c_n^1 & \text{if } c_n^1 \text{ possesses no links,} \\ c_n^1 & \text{if } c_n^1 \text{ is linked from } c_m^2 \text{ and } c_n^1 = c_m^2, \\ c_n^1 & \text{with probability } 1-g, \text{ if } c_n^1 \neq c_m^2, \\ c_m^2 & \text{with probability } g, \text{ if } c_n^1 \neq c_m^2. \end{cases} \tag{2}$$

The coupling operator $\hat{\mathbf{S}}$ is applied to network 2 simultaneously. Noteworthy, the links are not bidirectional coupling. For

example, if the cell c_n^1 is linked by c_m^2, c_m^2 may be linked by another arbitrary one in network 1, or even possess no links.

Different operator $\hat{\mathbf{R}}$ models different physical, biological, and artificial networks [4–16,31,35]. For two reasons, we take RBNs into consideration. First, the RBNs obeying the generalized totalistic rules for ECA can be described by a density map $p(t') = f(p(t), k)$, where $p(t')$ represents the probability of finding a cell in state 1 after $\hat{\mathbf{R}}$. For example, the map obeying generalized rule 126 is [18]

$$p(t') = 1 - p(t)^{k+1} - \big[1 - p(t)\big]^{k+1}, \tag{3}$$

where $k \geqslant 1$ is the number of connections of each cell. Besides being easy to deal with, the iteration formulation exhibits extremely bounteous chaotic behaviors. Actually, it is possible to extend the idea to other systems, such as the gene network [31] or the biological immune system [35]. Second, being similar with Conway's game of life, these totalistic RBNs have a natural interpretation in terms of the cell growth and ecology. In other words, they provide the simplified model to demonstrate the complexity in real systems.

Now the coupled model can be formulated progressively. Let $N_1^{1,2}(t)$ be the number of cell in state 1 and $N_0^{1,2}(t)$ be the number of cell in state 0 for two networks at time t. Obviously, they obey the conservation conditions

$$N_1^1(t) + N_0^1(t) = N_1^2(t) + N_0^2(t) = N \tag{4}$$

for all t. The first sub-step is to apply the free evolution operator to both networks. After being acted by $\hat{\mathbf{R}}$, $N_1^{1,2}$ turn out to be

$$N_1^{1,2}(t') = N f^{1,2}\big(p^{1,2}(t), k^{1,2}\big), \tag{5}$$

and evidently

$$N_0^{1,2}(t') = N\big[1 - f^{1,2}\big(p^{1,2}(t), k^{1,2}\big)\big]. \tag{6}$$

In the second sub-step, the stochastic coupling operator $\hat{\mathbf{S}}$ is applied. To simplify the description, we pay our attention to the network 1 and use the notation $f^{1,2}$ in place of $f^{1,2}(p^{1,2}(t), k^{1,2})$. For network 1, after being operated by $\hat{S}_n$ the number of cells staying in state 1 is

$$\begin{aligned} N_{1\to1}^1 &= N(1-\rho) f^1 + N\rho f^1 f^2 \\ &\quad + N\rho f^1\big(1 - f^2\big)(1-g). \end{aligned} \tag{7}$$

The first term in the right side of Eq. (6) corresponds to the situation that the cells possess no links from the network 2. The second term indicates the situation $(c_n^1, c_m^2) = (1, 1)$. The last term indicates $(c_n^1, c_m^2) = (1, 0)$ but the cells stay invariant with probability $1 - g$. Similarly, the number of cells changing their states from 1 to 0 is

$$N_{1\to0}^1 = N\rho f^1\big(1 - f^2\big)g, \tag{8}$$

where g is the probability that the cells become c_m^2. Using a similar argument as above, we can get the following results:

$$\begin{aligned} N_{0\to0}^1 &= N(1-\rho)\big(1 - f^1\big) + N\rho\big(1 - f^1\big)\big(1 - f^2\big) \\ &\quad + N\rho\big(1 - f^1\big) f^2(1-g), \end{aligned} \tag{9}$$

and

$$N_{0\to1}^1 = N\rho\big(1 - f^1\big) f^2 g. \tag{10}$$

One can check easily that $N_{1\to1}^1 + N_{1\to0}^1 + N_{0\to0}^1 + N_{0\to1}^1 = N$.

We can construct the coupled model by these equations. The probability of finding a cell in state 1 at time $t+1$ is given by

$$p^1(t+1) = \frac{N_{1\to1}^1 + N_{0\to1}^1}{N} = (1-\rho g) f^1 + \rho g f^2. \tag{11}$$

Repeating the procedure above, the density function for network 2 will become

$$p^2(t+1) = (1-\rho g) f^2 + \rho g f^1. \tag{12}$$

We call the multiplied term ρg the coupling strength ε. Thus, the final result is

$$\begin{cases} p^1(t+1) = (1-\varepsilon) f^1(p^1(t), k^1) + \varepsilon f^2(p^2(t), k^2), \\ p^2(t+1) = (1-\varepsilon) f^2(p^2(t), k^2) + \varepsilon f^1(p^1(t), k^1). \end{cases} \tag{13}$$

When $N \to \infty$, the two deterministic coupled polynomial maps can describe the density evolution of coupled RBNs regardless of the discrete nature of networks and the stochastic coupling methods.

In this Letter, we consider the RBNs which obey generalized Rule 22 for ECA. Like rule 126, rule 22 is another legal, totalistic, and complex rule among the 256 rules. Therefore, it can be simplified by a chaotic density map and has a natural interpretation in terms of the cell growth and ecological evolution [19]. Actually, the idea can also be applied to other totalistic rules.

By using the Boolean function, rule 22 becomes $f[0,0,1] = f[0,1,0] = f[1,0,0] = 1$, and $f = 0$ for the five remaining possible situations [2]. The density function is

$$p(t+1) = f\big(p(t), k\big) = (1+k)p(t)\big[1 - p(t)\big]^k, \tag{14}$$

and the details are shown in Appendix A. Fig. 1(a) illustrates the bifurcation diagram when $k \in R$. With the increase of k, the density map undergoes the route to chaos via period-doubling bifurcations. Fig. 1(b) shows the dependence of the Lyapunov exponent λ upon the chaotic parameter k. In terms of nonlinear dynamics, the Lyapunov exponent represents the convergence (divergence) properties of nearby trajectories. Divergence of trajectories along some direction in the phase space corresponds to a positive Lyapunov exponent, so $\lambda > 0$ suffices to ensure that the dynamics of the map is chaotic. The results correspond well with Fig. 1(a).

It is necessary to provide some numerical experiments to see if the model matches the original system. The graphs in Fig. 2 present the simulations of the polynomial model (mesh plot) and the actual coupled RBNs (points). Let $P(t) \equiv p^1(t) + p^2(t)$, we illustrate first two iterations $P(t+1)$, $P(t+2)$ versus $p^1(t)$, $p^2(t)$ individually for the case $N = 10^4$, $k^1 = k^2 = k = 12$, $\rho = 0.6$, and $g = 0.5$ ($\varepsilon = \rho g = 0.3$). Obviously, there is an excellent agreement between the coupled maps and the original system. If we increase the cell number N, the agreement will be improved correspondingly. For other parameter combinations, including the inhomogeneous situation $k^1 \neq k^2$, the model is still a very good approximation for the original system. The statement is examined by simulations for various parameters.

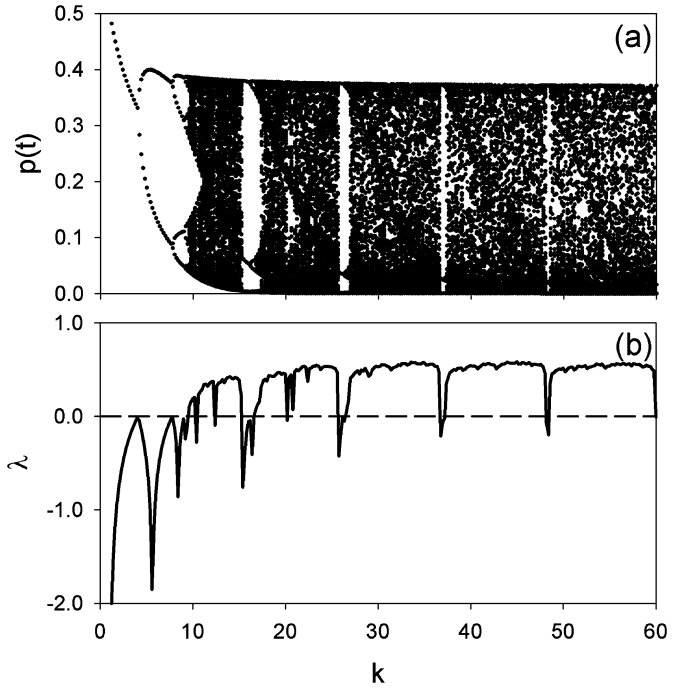

Fig. 1. Simulation results of the RBN based on generalized rule 22. (a) Illustrates the bifurcation diagram with $k \in R$, and (b) shows the dependence of the Lyapunov exponent λ on the parameter k.

3. Chaos synchronization

The investigation of chaos synchronization has been an important topic in nonlinear science owing to its various potential applications, such as secure communication [22], neuron systems [23], and the study of laser dynamics [24]. Synchronization can be regarded as the adjustment of the states of systems via the coupling. Depending on different coupling methods and coupling strengths, several different types of synchronization can be observed: complete synchronization (CS), phase synchronization (PS) [36], lag synchronization (LS) [37], anticipation synchronization [38], generalized synchronization (GS) [39] . . . , and so on. They represent the different degrees of correlation in interacting systems.

In this Letter, we study the chaos synchronization and interactive dynamics in coupled RBNs mentioned above. Choosing $N = 5 \times 10^4$, $k^1 = k^2 = k = 12$, $\rho = 0.9$, and the initial condition $(p^1(0), p^2(0)) = (0.1, 0.4)$, we plot the error evolution $e(t) \equiv |p^1(t) - p^2(t)|$ versus time for various exchanging probability g. Complete synchronization of two networks requires a fulfillment of the expression

$$\lim_{t\to\infty} e(t) = \lim_{t\to\infty} \left|p^1(t) - p^2(t)\right| = 0. \tag{15}$$

Fig. 3(a) presents the results when $g = 0$ (absence of coupling), two networks evolve in the asymptotically stable chaotic attractors individually and no synchronization is achieved. When $g = 0.1$, as shown in Fig. 3(b), the errors fluctuate around $e = 0.28$ with the pass of time. In the condition $g = 0.2$, the coupling is sufficient to overcome the divergent nature of nonlinearity, and the error converges toward zero. When g gets larger, the fluctuations decrease evidently, as shown in Fig. 3(d).

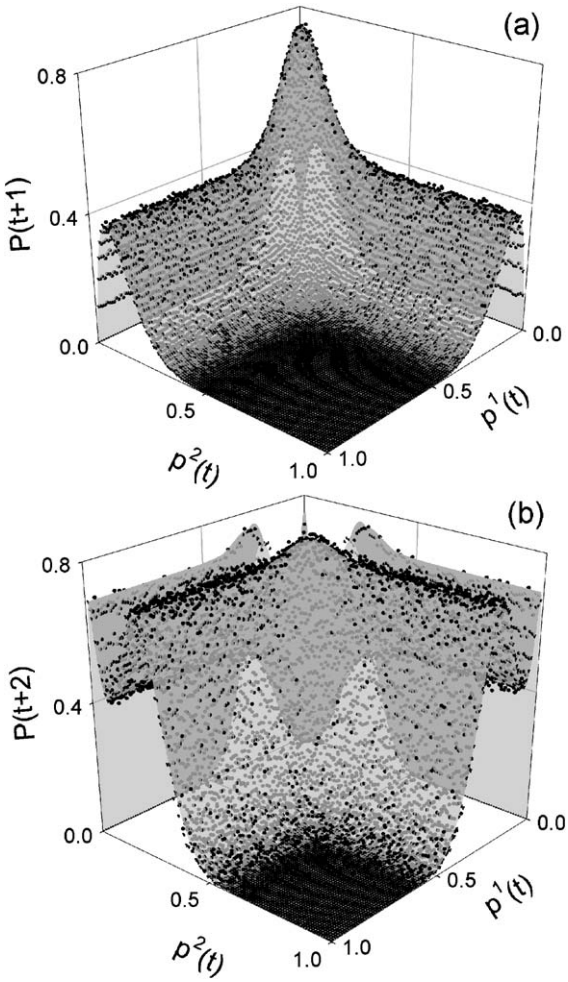

Fig. 2. The diagrams present the numerical results of the model (mesh plot) and the real coupled networks (points) with $N = 10^4$, $k^1 = k^2 = k = 12$, $\rho = 0.6$, and $g = 0.5$ ($\varepsilon = \rho g = 0.3$). The graphs (a) and (b) illustrate the first two iterations $P(t+1)$, $P(t+2)$ versus $p^1(t)$ and $p^2(t)$ individually.

To characterize the effects of coupling strength more clearly, we evaluate the mean-square error (*MSE*) between $p^1(t)$ and $p^2(t)$ with $\rho = 0.9$. The definition of *MSE* is that: $MSE = \frac{1}{n}\sum_{t=1}^{n} e(t)^2$. We show the relationships between *MSE* and coupling strength $\varepsilon = \rho g$ in Fig. 4(a) marked with empty circles. The complete synchronization occurs when the coupling parameter exceeds a critical value. For $\varepsilon \geqslant 0.18$, *MSE* approaches to zero and the CS is achieved. With ε getting larger, the synchronization is improved correspondingly. The results of density model, which tally well with the original system, are denoted by solid circles in the diagram simultaneously.

The dynamics of coupled RBNs can be easily realized by means of the coupled density maps. Choosing the identical parameters and initial conditions used above, Fig. 4(b) graphs the bifurcation diagrams for $p^1(t)$ versus different coupling strength. The bifurcations for $p^2(t)$ are identical to $p^1(t)$ except ε is extremely small (no represented). We can observe that the chaotic behaviors of $p^1(t)$ is suppressed gradually with the increase of the coupling strength when $\varepsilon \leqslant 0.06$. In the region $\varepsilon \in [0.06, 0.17]$, two systems are suppressed to be period-2. Even though the two coupled maps possess the same fixed

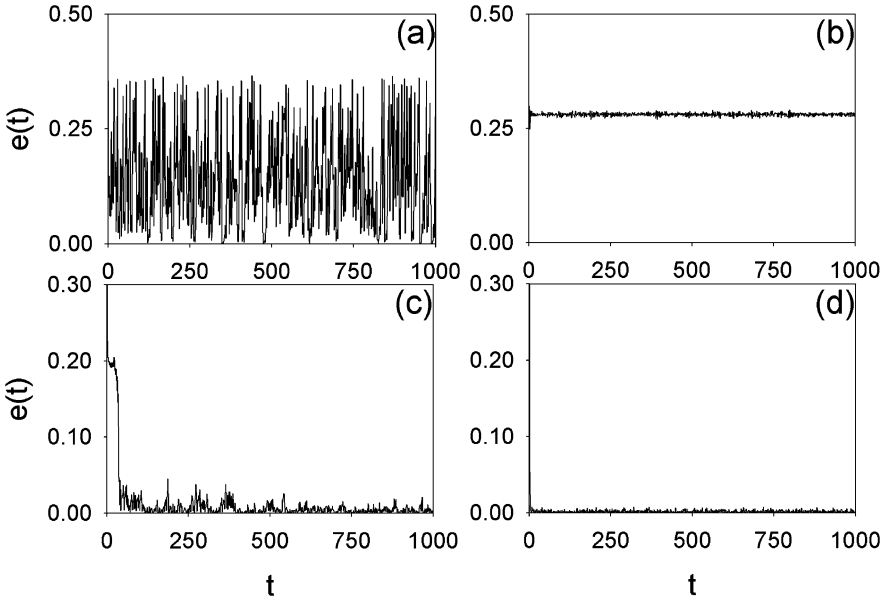

Fig. 3. The diagrams show the error evolution $e(t) \equiv |p^1(t) - p^2(t)|$ versus time for various exchanging probability g: (a) $g = 0.0$, (b) $g = 0.1$, (c) $g = 0.2$, and (d) $g = 0.4$.

points, they are in different phase. The values of *MSE* are then obtained easily via the values of the two fixed points in the bifurcation diagram. This is the reason that errors keep around $e = 0.28$ in Fig. 3(b). For $\varepsilon > 0.17$, chaos reappears and remains no matter what the value of ε is. The fact ensures that the synchronization phenomena in coupled RBNs are chaos synchronization. Finally, we analyze the dependence of the maximal Lyapunov exponent $\lambda_{\max}$ [40–42] on the coupling strength ε in Fig. 4(c). Comparing with the bifurcation diagrams, we can observe the excellent corresponding between them.

Based upon the concept of the diffusive synchronization stability matrix (DSSM) [43], we can determine the synchronization threshold analytically. The necessary condition for CS is $\lambda(k) + \ln(1 - 2\varepsilon) < 0$, where $\lambda(k)$ is the Lyapunov exponent of the uncoupled map. When $k = 12$, the coupling strengths in synchronization region (numerical results) satisfy the condition exactly ($\lambda(12) \cong 0.37$). Besides, we also investigate other conditions with different connectivity k. In Fig. 5, we show the *MSE* versus parameter pairs (k, ε), where $MSE = 0$ corresponds to the complete synchronization. Relying on the choice of k, CS will be achieved when coupling strength exceeds a corresponding critical value of coupling strength, which can be examined by DSSM.

Because the process of information exchange between networks may happen before individual evolution, it is possible to exchange the order of two operators in the update law. That is, Eq. (1) becomes

$$\mathbf{c}^{1,2}(t+1) = \hat{\mathbf{R}} \circ \hat{\mathbf{S}}\big(\mathbf{c}^{1,2}(t)\big). \tag{16}$$

Correspondingly, the coupled polynomial model can be reformulated as

$$\begin{cases} p^1(t+1) = f^1((1-\varepsilon)p^1(t) + \varepsilon p^2(t), k^1), \\ p^2(t+1) = f^2((1-\varepsilon)p^2(t) + \varepsilon p^1(t), k^2). \end{cases} \tag{17}$$

Though the dynamics of Eq. (17) differ from the previous coupled model, the chaos synchronization still can be observed. With the choice of parameters $k^1 = k^2 = k = 12$ and $(p^1(0), p^2(0)) = (0.1, 0.4)$, the *MSE* approaches to zero after $\varepsilon \geqslant 0.16$. In such regions, the individual network is chaotic and the largest Lyapunov exponent $\lambda_{\max}$ is larger than zero, as shown in Fig. 6.

4. Inhomogeneous condition

The systems consisting of identical elements are idealized and specialized cases because the subsystems in the realistic system are never the same. Therefore, the study of inhomogeneous condition has attracted a lot of attention [32–34]. In the recent days, Matache and Heidel consider a network consisting of several collections. The numbers of connections of nodes are identical in a collection, but they differ from each other when belonging to different collections. An interesting phenomenon is first observed in such inhomogeneous condition: the route to chaos is due to a cascade of period-doubling bifurcations which turn into period-halving bifurcations for certain parameter pairs [19]. A corresponding question thus arises: is the reverse process preserved in other systems, for example, the inhomogeneous coupled networks? In this Letter, the question is under our exploration.

The inhomogeneity here appears in the form of different connectivity values in each network. In other words, $k^1 \neq k^2$ in Eq. (13). To simplify the problem, we choose coupling strength $\varepsilon = 0.5$ which leads to $p^1(t) = p^2(t) \equiv p(t)$ after the first iteration. We plot the bifurcations of $p(t)$ with integer connectivity $k^1 = 3, 6, 9, 12, 15$ and the freely increasing k^2 in Fig. 7. The initial intensity values $(p^1(0), p^2(0))$ are all identical for each k^1. We can observe that the dynamics of system get more complex with the increase of k^1 and exhibit chaos after $k^1 \geqslant 9$. For $k^1 = 12$ and $k^1 = 15$, the period-doubling bifurcation start

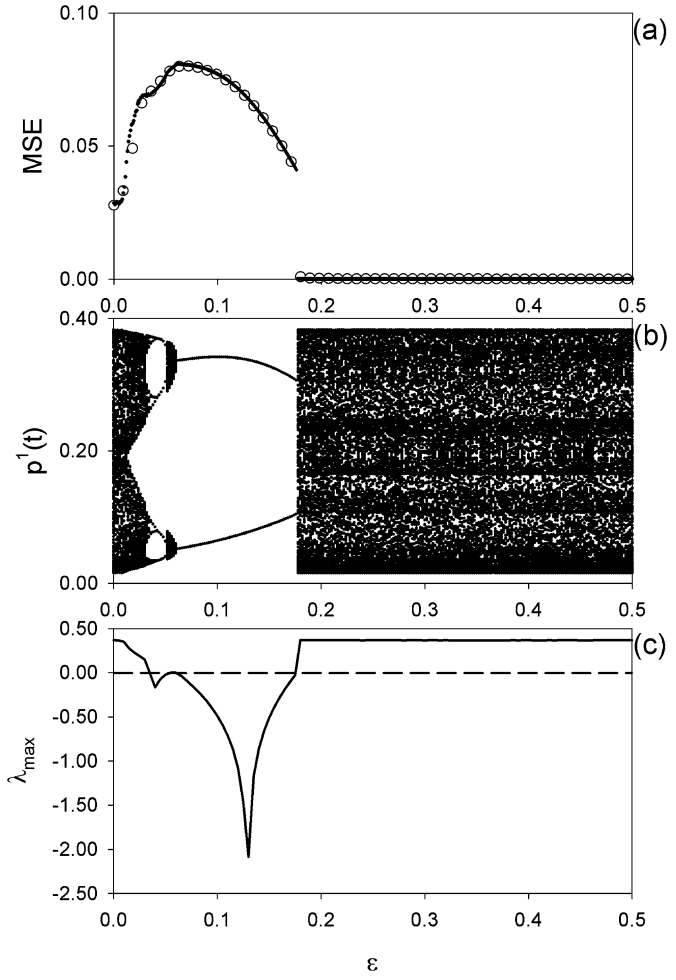

Fig. 4. In the condition $k^1 = k^2 = k = 12$, $\rho = 0.9$, and $(p^1(0), p^2(0)) = (0.1, 0.4)$. (a) The relationship between *MSE* and ε, where the results of the original system are denoted by empty circles and the results of model are denoted by solid circles. (b) The bifurcation diagrams of $p^1(t)$. The result of $p^2(t)$ is similar with $p^1(t)$. (c) The relationship between $\lambda_{\max}$ and the coupling strength ε.

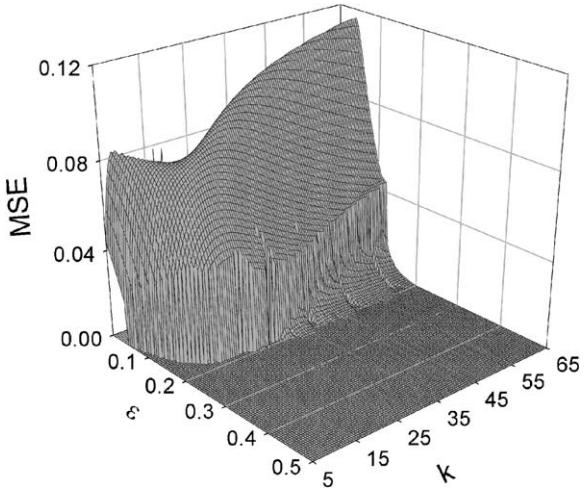

Fig. 5. The diagram shows the *MSE* versus various parameter pairs (k, ε), where $MSE = 0$ corresponds to the complete synchronization.

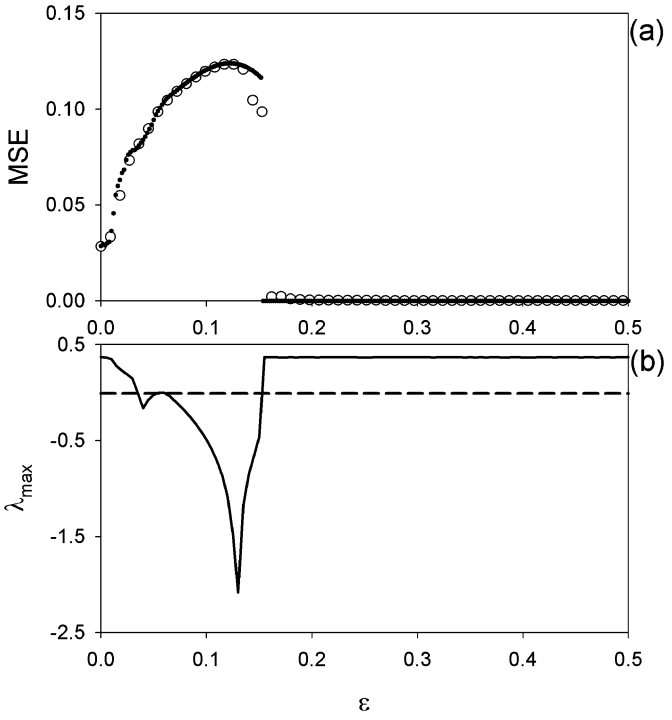

Fig. 6. In Eq. (17) with the choice of $k^1 = k^2 = k = 12$ and $(p^1(0), p^2(0)) = (0.1, 0.4)$, (a) shows the relationship between *MSE* and ε, where the results of original system are denoted by empty circles and the results of model are denoted by solid circles. (b) Shows the relationship between $\lambda_{\max}$ and the coupling strength ε.

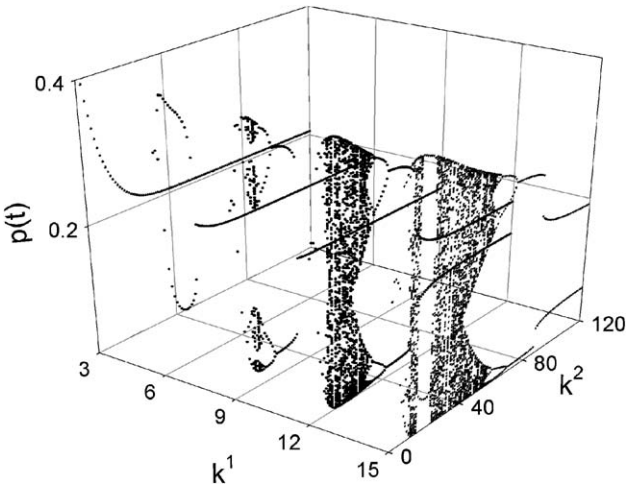

Fig. 7. The bifurcation diagrams of $p(t)$ as a function of k^1 and k^2. For $k^1 = 12$ and $k^1 = 15$, the period-doubling bifurcation start to reverse when k^2 exceed the critical point, and converge to period-2 finally.

to reverse when k^2 exceed the critical point, and converge to period-2 finally. To represent the dynamics more clearly, we illustrate the bifurcation diagram by holding $k^1 = 20$ and increasing k^2 in Fig. 8(a). The inset is a zoom-in view over a small range of k^2. Fig. 8(a) demonstrates that the system undergoes a cascade of period-doubling bifurcations to chaos, and reverses to periodical orbit via period-halving process. Similar reverse bifurcations are obtained for different choices of ε but with larger critical reversing point.

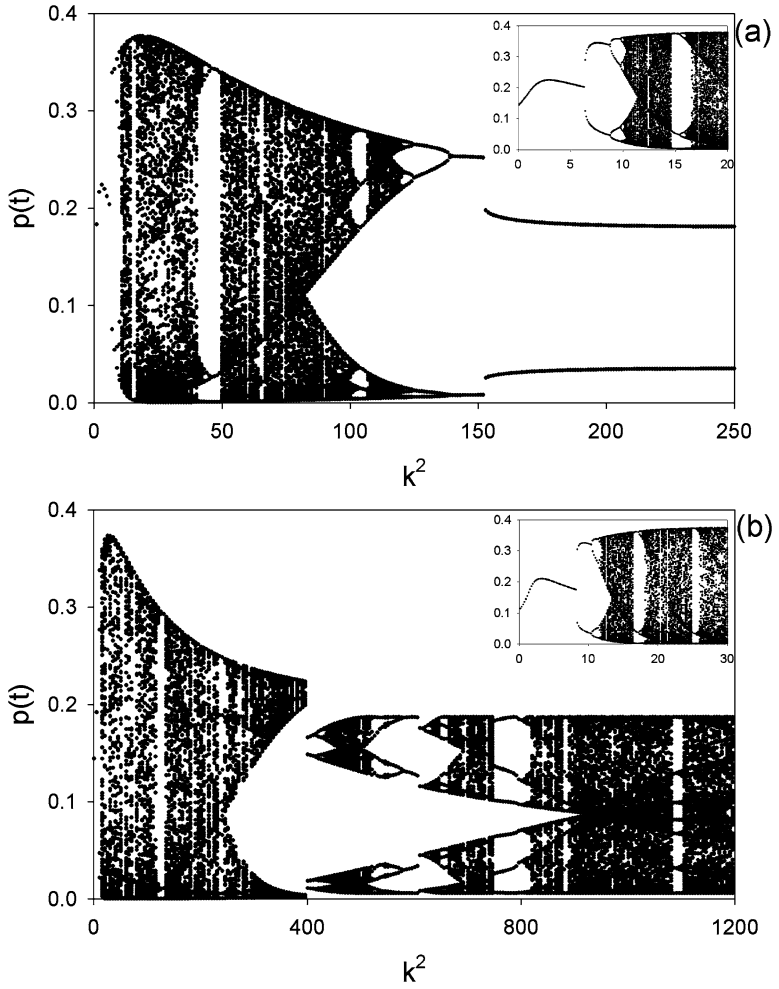

Fig. 8. The bifurcation diagrams of $p(t)$ for (a) $k^1 = 20$ and (b) $k^1 = 30$. The insets are zoom-in view over a small range of k^2.

For larger values of k^1, the situation become more complicated in our inhomogeneous model. Fig. 8(b) illustrates the bifurcation diagram in the case of $k^1 = 30$. In the region $1 \leqslant k^2 \leqslant 398$, the system undergoes the route to chaos and then starts to reverse immediately. However, after $k^2 > 398$ the system goes through another sequence of period-doubling bifurcations and exhibits chaotic behavior once again. Similar results can be noted effortlessly for $k^1 \geqslant 25$.

To understand the mechanism of reverse bifurcation stated above, we take the limit $k^2 \to \infty$ and reformulate Eq. (13) as

$$\begin{cases} p^1(t+1) = (1-\varepsilon) f^1(p^1(t), k^1), \\ p^2(t+1) = \varepsilon f^1(p^1(t), k^1). \end{cases} \tag{18}$$

Choosing coupling strength $\varepsilon = 0.5$, the equations then reduce to be

$$p^1(t) = p^2(t) = p(t) = \frac{1}{2}\big(1+k^1\big)p(t)\big[1-p(t)\big]^{k^1}, \tag{19}$$

which characters the dynamical behaviors of inhomogeneous model for large k^2. The bifurcation diagram and Lyapunov exponent λ of reduced map (19) are represented in Fig. 9. In the region $0 \leqslant k \leqslant 11.5$, the attractor is a stable fixed point (period-1) and for $11.5 < k \leqslant 21$ is a stable period-2 cycle. This is the reason that the system converge to periodic orbit when k^2 exceed a critical point in Figs. 7 and 8(a). For $k \geqslant 25$, the reduced map becomes chaotic and thus results in the reappearance of period-doubling bifurcations, as illustrated in Fig. 8(b). Noteworthy, when k^1 locates at the periodic window in Fig. 9, the system requires much larger value of k^2 to reach the final periodic state (not represented). Owing to the instability, the process of period-halving is relatively hard to be observed.

It is possible to investigate the inhomogeneity in the form of entirely different evolution rule [34], for example, one network obeys rule 22 and the other obeys rule 126. The results will be presented in our further works where we will generalize the coupling mechanism to couple more than two RBNs.

5. Conclusions

We study the dynamics of two stochastically coupled random Boolean networks (RBNs) in this Letter. Due to the "site-by-site and all to all" coupling is relatively uncommon in real systems, we modify the coupling scheme to model co-evolution of biological species via horizontal genetic exchange. We show that the density evolution of networks can be described by two deterministic coupled polynomial maps, even thought the systems are stochastically coupled. Our model provides good

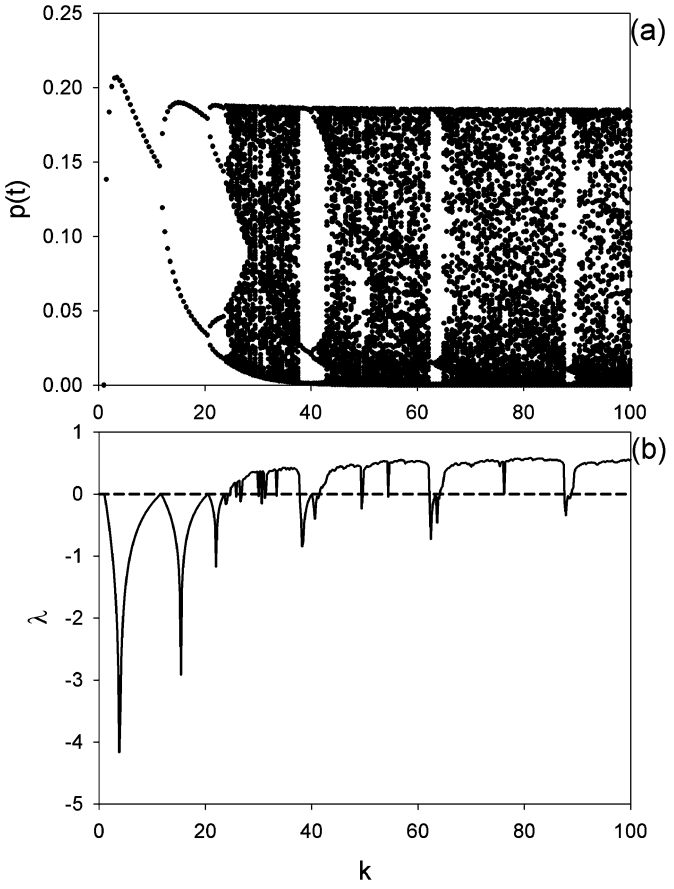

Fig. 9. Simulation results of the reduced map in Eq. (19). (a) Shows the bifurcation diagram, and (b) shows the dependence of the maximal Lyapunov exponent λ on the parameter k.

predictions and analytical calculations of the original networks. Moreover, we study the inhomogeneous condition in the form of different values of connectivity in each network. The reverse bifurcations via period-halving process are under our analysis and discussion.

Acknowledgements

The authors would like to thank the National Science Council, Taiwan, ROC, for financially supporting this research under Contract No. NSC 94-2112-M-017-003.

Appendix A. Derivation of density map for rule 22

In this appendix, we formulate the density map to describe the dynamical behavior of a generalized RBN based on rule 22.

Consider a RBN with N cells ($N \to \infty$). Each cell c_n, where $n = 1, 2, \ldots, N$, is described by two values 1 or 0. The connections of a cell c_n could be assigned randomly from its belonged network, and the number of connections is denoted by k fixed for all cells during evolution. The generalized evolution rule 22 is as follows:

$$c_n(t+1) = \begin{cases} 1, & [c_n(t) + S_{nk}(t)] = 1, \\ 0, & \text{otherwise}, \end{cases} \tag{A.1}$$

where $S_{nk} = \sum_{j=1}^{k} c_{nj}(t)$ is the sum of the k random connections of cell c_n.

The density of the RBN at time t is given by $p(t) = N^{-1} \sum_{n=1}^{N} c_n(t)$. Of course, the density also satisfies with $p(t) = N_1/(N_0 + N_1)$, where N_1 is the number of cells in state 1 and N_0 is the number of cells in state 0 at time t. After being operated by evolution rule, the number of cells that are 1 at time t and remain 1 at time $t+1$ is given by

$$N_{1\to1}(t) = N_1\big[1 - p(t)\big]^k. \tag{A.2}$$

Similarly, we can get the number of cells that change their states from 1 to 0:

$$N_{1\to0}(t) = N_1\big\{1 - \big[1 - p(t)\big]^k\big\}. \tag{A.3}$$

The number of cells that change their states from 0 to 1:

$$\begin{aligned} N_{0\to1}(t) &= N_0 \binom{k}{1} p(t)\big[1 - p(t)\big]^{k-1} \\ &= N_0 k p(t)\big[1 - p(t)\big]^{k-1}, \end{aligned} \tag{A.4}$$

and the number of cells that keep their states 0:

$$N_{0\to0}(t) = N_0\big\{1 - kp(t)\big[1 - p(t)\big]^{k-1}\big\}. \tag{A.5}$$

Inserting the results from Eqs. (2) and (4) into $p(t+1)$, then we can get Eq. (14).

References

[1] S. Wolfram, Rev. Mod. Phys. 55 (1983) 601.
[2] S. Wolfram, Cellular Automata and Complexity, Addison–Wesley, New York, 1994.
[3] S. Wolfram, A New Kind of Science, Wolfram Media, Champaign, 2002.
[4] T. Toffoli, N. Margolus, Cellular Automata Machines: A New Environment for Modeling, MIT Press, Cambridge, MA, 1987.
[5] B. Chopard, M. Droz, Cellular Automata Modeling of Physical Systems, Cambridge Univ. Press, Cambridge, 1998.
[6] G. Vichniac, Physica D 10 (1984) 96.
[7] B. Chopard, P. Luthi, M. Droz, Phys. Rev. Lett. 72 (1994) 1384.
[8] A.K. Gunstensen, D.H. Rothman, S. Zaleski, G. Zanetti, Phys. Rev. A 43 (1991) 4320.
[9] J. Gravner, D. Griffeath, Adv. Appl. Math. 21 (1998) 241.
[10] B.H. Wang, L. Wang, P.M. Hui, B. Hu, Int. J. Nonlinear Sci. Numer. Simul. 1 (4) (2000) 255.
[11] D. Mao, B.H. Wang, L. Wang, P.K. Hui, C.K. Hu, Int. J. Nonlinear Sci. Numer. Simul. 4 (3) (2003) 239.
[12] S.A. Kauffman, J. Theor. Biol. 22 (1969) 437.
[13] S.A. Kauffman, The Origins of Order, Oxford Univ. Press, Cambridge, 1993.
[14] B. Derrida, Y. Pomeau, Europhys. Lett. 1 (1986) 45.
[15] B. Derrida, G. Weisbuch, J. Phys. (Paris) 47 (1986) 1297.
[16] H. Flyvbjerg, J. Phys. A 21 (1988) L955.
[17] L.G. Morelli, D.H. Zanette, Phys. Rev. E 63 (2001) 036204.
[18] M. Andrecut, M.K. Ali, Int. J. Mod. Phys. B 15 (2001) 17.
[19] M.T. Matache, J. Heidel, Phys. Rev. E 69 (2004) 056214.
[20] M.T. Matache, J. Heidel, Phys. Rev. E 71 (2005) 026232.
[21] L. Pecora, T. Carroll, Phys. Rev. Lett. 64 (1990) 821.
[22] U. Parlitz, L. Kocarev, T. Stojanovski, H. Preckel, Phys. Rev. E 53 (1996) 4351.
[23] J.W. Shuaim, K.W. Wong, Phys. Rev. E 57 (1998) 7002.
[24] R. Roy, K.S. Thornburg Jr., Phys. Rev. Lett. 72 (1994) 2009.
[25] M.C. Ho, Y.C. Hung, Phys. Lett. A 301 (2002) 424.
[26] L.G. Morelli, D.H. Zanette, Phys. Rev. E 58 (1998) R8.

[27] L.G. Morelli, D.H. Zanette, Phys. Rev. E 63 (2001) 036204.
[28] M.C. Ho, Y.C. Hung, I.M. Jiang, Phys. Lett. A 344 (2005) 36.
[29] T. Ohtomo, K. Otsuka, A. Okamoto, J.-Y. Ko, Opt. Express 13 (2005) 358.
[30] M.C. Maiden, FEMS Microbiol. Lett. 112 (3) (1993) 243.
[31] J.A. de Sales, M.L. Martins, D.A. Stariolo, Phys. Rev. E 55 (1997) 3262.
[32] R.O. Grigoriev, M.C. Cross, H.G. Schuster, Phys. Rev. Lett. 79 (1997) 2795.
[33] A. Sharma, N. Gupte, Phys. Rev. E 66 (2002) 036210.
[34] M.C. Ho, Y.C. Hung, I.M. Jiang, Phys. Lett. A 324 (2004) 450.
[35] T. Tomé, J.R. Drugowich de Felício, Phys. Rev. E 53 (1996) 3976.
[36] M.G. Rosenblum, A.S. Pikovsky, J. Kurths, Phys. Rev. Lett. 76 (1996) 1804;
E. Rosa, E. Ott, M.H. Hess, Phys. Rev. Lett. 80 (1998) 1642.
[37] S. Taherion, Y.C. Lai, Phys. Rev. E 59 (1999) R6247.
[38] H.U. Voss, Phys. Rev. E 61 (2000) 5115.
[39] T.L. Carroll, J.F. Heagy, L.M. Pecora, Phys. Rev. E 54 (1996) 4676;
L. Kocarev, U. Parlitz, Phys. Rev. Lett. 76 (1996) 1816.
[40] S. Morita, Phys. Lett. A 226 (1997) 172.
[41] A.M. Batista, R.L. Viana, Phys. Lett. A 286 (2001) 134.
[42] A.M. Batista, S.E. de S. Pinto, R.L. Viana, S.R. Lopes, Phys. Rev. E 65 (2002) 056209.
[43] A. Stefański, J. Wojewoda, T. Kapitaniak, S. Yanchuk, Phys. Rev. E 70 (2004) 026217.